A detection instrument for enhanced-fluorescence and label-free imaging on photonic crystal surfaces

Ian D. Block,[1†] Patrick C. Mathias,[2†] Nikhil Ganesh,[3†] Sarah I. Jones,[4] Brian R. Dorvel,[5†] Vikram Chaudhery,[1†] Lila O. Vodkin,[4] Rashid Bashir,[1,2†] and Brian T. Cunningham[1†*]

[1]*Dept. of Electrical Engineering, University of Illinois at Urbana-Champaign, Urbana, IL, USA*
[2]*Dept. of Bioengineering, University of Illinois at Urbana-Champaign, Urbana, IL, USA*
[3]*Dept. of Materials Science and Engineering, University of Illinois at Urbana-Champaign, Urbana, IL, USA*
[4]*Dept. of Crop Sciences, University of Illinois at Urbana-Champaign, Urbana, IL, USA*
[5]*Dept. of Biophysics and Computational Biology, University of Illinois at Urbana-Champaign, Urbana, IL, USA*
[†]*Micro and Nanotechnology Laboratory, University of Illinois at Urbana-Champaign, Urbana, IL USA*
[*]*bcunning@illinois.edu*

Abstract: We report on the design and demonstration of an optical imaging system capable of exciting surface-bound fluorophores within the resonant evanescent electric field of a photonic crystal surface and gathering fluorescence emission that is directed toward the imaging objective by the photonic crystal. The system also has the ability to quantify shifts in the local resonance angle induced by the adsorption of biomolecules on the photonic crystal surface for label-free biomolecular imaging. With these two capabilities combined within a single detection system, we demonstrate label-free images self-registered to enhanced fluorescence images with 328x more sensitive fluorescence detection relative to a glass surface. This technique is applied to a DNA microarray where label-free quantification of immobilized capture DNA enables improved quality control and subsequent enhanced fluorescence detection of dye-tagged hybridized DNA yields 3x more genes to be detected versus commercially available microarray substrates.

OCIS codes: (280.1415) Biological sensing and sensors; (050.5298) Photonic crystals; (180.2520) Fluorescence microscopy

References and links

1. K. H. Drexhage, "Influence of a dielectric interface on fluorescence decay time," J. Luminescence **1**, 693-701 (1970).
2. J. R. Lakowicz, "Radiative decay engineering 5: metal-enhanced fluorescence and plasmon emission," Anal. Biochem. **337**, 171-194 (2005).
3. C. D. Geddes and J. R. Lakowicz, "Metal-Enhanced Fluorescence," J. Fluorescence **12**, 121-129 (2002).
4. B. Rothenhausler and W. Knoll, "Surface-plasmon microscopy," Nature **332**, 615-617 (1988).
5. A. W. Wark, H. J. Lee, and R. M. Corn, "Advanced Methods for SPR Biosensing," in *Handbook of Surface Plasmon Resonance*, R. B. M. Schasfoort and A. J. Tudos, eds. (RSC Publishing, London, 2008), pp. 251-280.
6. Y. Arima, Y. Teramura, H. Takiguchi, K. Kawano, H. Kotera, and H. Iwata, "Surface plasmon resonance and surface plasmon field-enhanced fluorescence spectroscopy for sensitive detection of tumor markers," Meth. Molec. Bio. **503**, 3-20 (2009).
7. P. Anger, P. Bharadwaj, and L. Novotny, "Enhancement and quenching of single-molecule fluorescence," Phys. Rev. Lett. **96**, 113002 (2006).
8. T. Shtoyko, E. G. Matveeva, I.-F. Chang, Z. Gryczynski, E. Goldys, and I. Gryczynski, "Enhanced fluorescent immunoassays on silver factal-like structures," Anal. Chem. **80**, 1962-1966 (2008).
9. T. M. Chinowsky, T. Mactutis, E. Fu, and P. Yager, "Optical and electronic design for a high-performance surface plasmon resonance imager," Proc. SPIE **5261**, 173-182 (2004).

#112354 - $15.00 USD Received 5 Jun 2009; revised 9 Jul 2009; accepted 11 Jul 2009; published 17 Jul 2009

10. B. T. Cunningham and e. al, "Label-Free Assays on the BIND System," J. Biomolec. Screening **9**, 481-490 (2004).
11. B. T. Cunningham and L. L. Laing, "Label-free detection of biomolecular interactions: Applications in proteomics and drug discovery," Expert Reviews in Proteomics **3**, 271-281 (2006).
12. B. Lin, P. Li, and B. T. Cunningham, "A Label-Free Biosensor-Based Cell Attachment Assay for Characterization of Cell Surface Molecules," Sens. Actuators B **114**, 559-564 (2006).
13. L. L. Chan, M. F. Pineda, J. Heeres, P. Hergenrother, and B. T. Cunningham, "General method for discovering inhibitors of protein-DNA interactions using photonic crystal biosensors," ACS Chem. Bio. **3**, 437-448 (2008).
14. N. Ganesh, I. D. Block, and B. T. Cunningham, "Near ultraviolet-wavelength photonic-crystal biosensor with enhanced surface-to-bulk sensitivity ratio," Appl. Phys. Lett. **89**, 023901 (2006).
15. N. Ganesh, A. Xiang, N. B. Beltran, D. W. Dobbs, and B. T. Cunningham, "Compact wavelength detection system incorporating a guided-mode resonance filter," Appl. Phys. Lett. **90**, 081103-081106 (2007).
16. P. Li, B. Lin, J. Gerstenmaier, and B. T. Cunningham, "A new method for label-free imaging of biomolecular interactions," Sens. Actuators B, Chemical **99**, 6-13 (2004).
17. L. L. Chan, P. Y. Li, D. Puff, and B. T. Cunningham, "A Self-Referencing Method for Microplate Label-Free Photonic Crystal Biosensors," IEEE Sensors **6**, 15510-11556 (2006).
18. C. J. Choi and B. T. Cunningham, "A 96-sell microplate incorporating a replica molded microfluidic network integrated with photonic crystal biosensors for high throughput kinetic biomolecular interaction analysis," Lab On A Chip **7**, 550-556 (2007).
19. L. Chan, S. Gosangari, K. Watkin, and B. T. Cunningham, "A label-free photonic crystal biosensor imaging method for detection of cancer cell cytotoxicity and proliferation," Apoptosis **12**, 1061-1068 (2007).
20. L. L. Chan, S. Gosangari, K. L. Watkin, and B. T. Cunningham, "Label-free imaging of cancer cells using photonic crystal biosensors and application to cytotoxicity screening of a natural compound library," Sens. Actuators B **132**, 418-425 (2008).
21. D. Neuschaefer, W. Budach, C. Wanke, and S.-D. Chibout, "Evanescent resonator chips: a universal platform with superior sensitivity for fluorescence-based microarrays," Bio. Bioelectron. **18**, 489-497 (2003).
22. N. Ganesh, P. C. Mathias, W. Zhang, and B. T. Cunningham, "Distance dependence of fluorescence enhancement from photonic crystal surfaces," Journal of Applied Physics **103**, 083104 (2008).
23. P. C. Mathias, N. Ganesh, W. Zhang, and B. T. Cunningham, "Graded Wavelength One-Dimensional Photonic Crystal Reveals Spectral Characteristics of Enhanced Fluorescence," J. Appl. Phys. **103**, 094320 (2008).
24. P. C. Mathias, N. Ganesh, and B. T. Cunningham, "Application of photonic crystal enhanced fluorescence to a cytokine immunoassay," Anal. Chem. **80**, 9013-9020 (2008).
25. P. C. Mathias, N. Ganesh, L. L. Chan, and B. T. Cunningham, "Combined enhanced fluorescence and label-free biomolecular detection with a photonic crystal surface," Appl. Opt. **46**, 2351-2360 (2007).
26. N. Ganesh, W. Zhang, P. C. Mathias, E. Chow, J. A. N. T. Soares, V. Malyarchuk, A. D. Smith, and B. T. Cunningham, "Enhanced fluorescence emission from quantum dots on a photonic crystal surface," Nature Nanotechnol. **2**, 515-520 (2007).
27. P. C. Mathias, H.-Y. Wu, and B. T. Cunningham, "Employing two distinct photonic crystal resonances for improved fluorescence enhancement," Appl. Phys. Lett. (to be published).
28. N. Ganesh, I. D. Block, P. C. Mathias, W. Zhang, V. Malyarchuk, and B. T. Cunningham, "Leaky-mode assisted fluorescence extraction: application to fluorescence enhancement biosensors," Opt. Express **16**, 21626-21640 (2008).
29. W. Zhang, I. Shmulevich, and J. Astola, *Microarray Quality Control* (Wiley, Hoboken, 2004).
30. B. T. Cunningham, B. Lin, J. Qiu, P. Li, J. Pepper, and B. Hugh, "A plastic colorimetric resonant optical biosensor for multiparallel detection of label-free biochemical interactions," Sens. Actuators B **85**, 219-226 (2002).
31. I. D. Block, N. Ganesh, M. Lu, and B. T. Cunningham, "A sensitivity model for predicting photonic cyrstal biosensor performance," IEEE Sensors **8**, 274-280 (2008).
32. B. Dorvel, B. R. Jr., I. D. Block, P. C. Mathias, S. E. Clare, D. E. Bergstrom, B. T. Cunningham, and R. Bashir, "Vapor phase deposition of monofunctional alkoxysilanes for sub-nanometer level biointerfacing on oxide surfaces," Adv. Functional Mater. (under review).
33. L. S. Jung, C. T. Campbell, T. M. Chinowsky, M. N. Mar, and S. S. Yee, "Quantitative interpretation of the response of surface plasmon resonance sensors to adsorbed films," Langmuir **14**, 5636-5648 (1998).
34. J. S. Shumaker-Parry and C. T. Campbell, "Quantitative methods for spatially resolved adsorption/desorption measurements in real time by surface plasmon resonance microscopy," Anal. Chem. **76**, 907-917 (2004).
35. X. Zhu, J. P. Landry, Y.-S. Sun, J. P. Gregg, K. S. Lam, and X. Guo, "Oblique-incidence reflectivity difference microscope for label-free high-throughput detection of biochemical reactions in a microarray format," Appl. Opt. **46**, 1890-1895 (2007).
36. E. Ozkumur, J. W. Needham, D. A. Bergstein, R. Gonzalez, M. Cabodi, J. M. Gershoni, B. B. Goldberg, and M. S. Unlu, "Label-free and dynamic detection of biomolecular interactions for high-throughput microarray applications," PNAS **105**, 7988-7992 (2008).

#112354 - $15.00 USD Received 5 Jun 2009; revised 9 Jul 2009; accepted 11 Jul 2009; published 17 Jul 2009

37. E. Fu, T. Chinowsky, J. Foley, J. Weinstein, and P. Yager, "Characterization of a wavelength-tunable surface plasmon resonance microscope," Rev. Scie. Instruments **75**, 2300-2304 (2004).
38. Y.-J. Hung, I. I. Smolyaninov, C. C. Davis, and H.-C. Wu, "Fluorescence enhancement by surface gratings," Opt. Express **14**, 10825-10830 (2006).
39. C. R. Sabanayagam and J. R. Lakowicz, "Increasing the sensitivity of DNA microarrays by metal-enhanced fluorescence using surface-bound silver nanoparticles," Nucleic Acids Research **35**, e13 (2007).
40. E. L. Moal, E. Fort, S. Leveque-Fort, F. P. Cordelieres, M.-P. Fontaine-Aupart, and C. Ricolleau, "Enhanced fluorescence cell imaging with metal-coated slides," Biophys. J. **92**, 2150-2161 (2007).
41. L. Shi, "The Microarray Quality Control (MAQD) project shows inter- and intraplatform reproducibility of gene expression measurements," Nature Biotechnol. **24**, 1151-1161 (2006).
42. A. W. Peterson, R. J. Heaton, and R. M. Georgiadis, "The effect of surface probe density on DNA hybridization," Nucleic Acids Research **29**, 5163-5168 (2001).
43. D. S. Dandy, P. Wu, and D. W. Grainger, "Array feature size influences nucleic acid surface capture in DNA microarrays," PNAS **104**, 8223-8228 (2007).

1. Introduction

Fluorescence has emerged as the most attractive imaging and detection technique across the life sciences due to its excellent sensitivity and specificity as well as the low cost and flexibility of the method. While fluorescence is a very sensitive technique, weak signals often limit visualization and quantitation of low abundance molecules in the context of gene expression analysis, biomarker detection and cellular imaging. To maximize the sensitivity of these methods, a variety of metallic surfaces have been studied for the purpose of enhancing fluorescence output. An extensive literature has evolved since pioneering work in the field several decades ago [1] and numerous reviews exist summarizing recent progress [2, 3]. Enhancement is reported to arise from several effects, including locally intense optical fields, reduced fluorescence lifetimes, and directional emission.

Surface plasmons supported by metal surfaces, in part responsible for metal enhanced fluorescence, can also be used for imaging of surface-based molecular interactions without the use of any fluorescent tags [4]. While the sensitivity of surface plasmon resonance (SPR) imaging is typically orders of magnitude lower than for fluorescence imaging, the ability to detect biomolecular interactions in real time without labeling has resulted in its widespread adoption for numerous applications in biomolecular affinity studies [5]. The technique has also been combined recently with metal enhanced fluorescence in a preliminary effort to detect tumor markers [6].

While metallic surfaces have shown great promise for enhancing the output of surface-bound fluorophores, they have been limited by quenching of emission near to the surface [7], "hotspotting" leading to poor reproducibility and uniformity [8], and prism coupling setups that limit image size and throughput. Similarly for SPR imaging, broad resonances limit the sensitivity, a tilted object plane restricts the quality of focus and field of view [9], and cumbersome prism-coupling schemes hinder the practicality of robust, high-throughput label-free imaging. In an effort to overcome these limitations, we have pursued the application of photonic crystal (PC) surfaces to both enhanced fluorescence (EF) and label-free (LF) imaging.

PC surfaces that are designed to produce narrowband resonant reflections at specific wavelengths have been demonstrated for applications in label-free biosensing [10-13] in which the resonant wavelength may be designed to occur at wavelengths spanning the ultraviolet [14] to infrared [15] by selection of the PC period, the refractive index of the PC materials, and the vertical dimensions of the grating structure. Due to the strong spatial confinement of resonant light in the plane of the PC surface, label-free imaging of biomolecules [16-18] and cells [19, 20] has also been demonstrated. While devices for label-free imaging utilize the far-field reflectance behavior of the PC, in which nearly 100% reflection efficiency is obtained at the resonant wavelength, recent structures have been designed to take advantage of the near-field properties of the PC. Electric fields associated

#112354 - $15.00 USD Received 5 Jun 2009; revised 9 Jul 2009; accepted 11 Jul 2009; published 17 Jul 2009

with resonant reflection are confined within the PC and evanescent into the adjacent media and are strongly enhanced with respect to the electric field of the external illumination source [21, 22]. By spectrally aligning a PC resonant mode with the laser used to excite fluorescent dyes, one can achieve an increase in the emission intensity of the dye in comparison to the same fluorophore excited on a plain glass surface [23]. Previous publications have shown the "enhanced excitation" amplification factor of a PC to be ~6x using a confocal laser scanning instrument. This has aided in achieving detection of the protein biomarker tumor necrosis factor alpha down to 120 fg/ml, more than one order of magnitude lower than that detected by standard methods (unpublished follow-up data to previous work) [24].

PC surfaces have also been demonstrated that are capable of simultaneously providing resonant reflections at multiple wavelengths, using structures with different periodic modulations in two orthogonal directions [25]. 1-dimensional PCs (i.e. comprised of a linear grating surface structure) may also produce resonant reflections at two distinct wavelengths either by illumination at an off-normal angle of incidence (in which the PC dispersion splits, and the resonant wavelengths diverge with increasing incident angle) [26], or by utilizing separate Transverse Electric (TE) and Transverse Magnetic (TM) modes [27]. The additional resonance may be chosen to coincide with the emission spectrum of a surface-adsorbed fluorophore and engineered to redirect fluorescence emission toward a detector oriented normal to the PC surface [28]. This "enhanced extraction" phenomenon provides a mechanism for improving the collection efficiency of fluorescence emission that would have been emitted obliquely and missed by the finite collection aperture or otherwise lost to substrate-guided modes. Enhanced extraction has been shown to produce a 4.8x increase in photon collection efficiency compared to detection from the same fluorophores emitting on an unpatterned glass surface, again using a confocal laser scanner as a detection instrument [27]. When a PC is designed to produce resonant reflections at both the excitation wavelength and emission wavelength of a fluorophore, the effects of both gain mechanisms multiply, resulting in up to 60x magnification of overall fluorescence signal.

In our previous work, a commercially available confocal laser scanner was used for providing laser illumination of PC surfaces for enhanced fluorescence. We have also previously demonstrated a label-free imaging detection instrument that is capable of measuring the spatial distribution of PC resonance shifts due to adsorption of biomolecules and cells with pixel resolution as small as 6x6 μm^2 [16]. However, our goal in this work was to design and demonstrate an imaging instrument optimized for both EF and LF imaging, while overcoming limitations (in sensitivity and resolution) of both previously employed instruments. Due to the inflexibility of the commercial laser scanner in terms of laser illumination angle, laser wavelength, imaging spatial resolution, and fluorophore collection optics, we sought to design a widefield imaging system using collimated angle-tunable laser illumination. This design enables imaging of a photonic crystal surface using the same illumination source and imaging optics for both EF and LF modalities. Using this approach, high-resolution and high-sensitivity LF and EF images may be accurately registered with each other for application in several important areas of life science research, diagnostic testing, and drug discovery.

In general, label-free biosensor imaging methods do not offer the same level of sensitivity as fluorescence-based methods. However, for most fluorescent surface-based assays, there is no mechanism for quantification of the density of immobilized capture ligand. This capability is especially important for the production of DNA and protein microarrays that are produced by pin-spotting or piezoelectric jet spotting because a large variability exists in spot size and density [29]. The ability to perform LF imaging of immobilized ligand spots would potentially provide a quality control tool for elimination of missing spots or spots with poor characteristics (in terms of density, size, or uniformity) to improve the reliability of microarrays for disease diagnostics based upon detection of expressed genes or protein biomarkers. Because the immobilized spot density is typically high, detection by LF methods

#112354 - $15.00 USD Received 5 Jun 2009; revised 9 Jul 2009; accepted 11 Jul 2009; published 17 Jul 2009

does not pose a difficult sensitivity challenge, although sufficient spatial resolution is required for imaging capture spots that are 50-200 μm in diameter. Therefore, one application of this technology is the detection of capture spots in LF mode and subsequent detection of fluorescent-tagged analytes in EF mode, where the highest possible level of sensitivity is desired.

In this work we first characterize the sensitivity of LF and EF imaging using a PC surface optimized for use with the combined EF and LF imaging instrument. Using strepavidin-Cy5, we demonstrate LF images self-registered to fluorescence images on a PC having 328x fluorescence enhancement measured relative to a standard glass slide. We then use a microarray printed on a PC to demonstrate the potential utility of LF imaging for quality control of DNA capture spots. We also show the benefits of the registered EF image of hybridized labeled DNA in achieving a three-fold improvement in the number of genes detected relative to a glass substrate.

2. Instrumentation and Device Design

A schematic drawing of the LF/EF imaging microscope is shown in Fig. 1. A 35mW HeNe laser chosen to align with the excitation spectrum of the fluorescent dye cyanine-5 (Cy5) passes through a half-wave plate (for polarization control), a variable neutral density filter, a rotating diffuser (to reduce speckle and fringes at the imaging plane due to spatial coherence), a 10x beam expander, an aperture, and a motorized angle-tunable mirror. The gimbal-mounted mirror sits on top of a motorized linear stage in order to maintain a constant illumination area on the device as the mirror rotates. The remainder of the imaging path makes use of an Olympus BX-51 upright microscope with a Cy5 filter cube (Semrock) and a variety of objectives. Several important features make this implementation ideal for combined EF and LF imaging. First, it uses a common beam-path for both imaging modes, facilitating acquisition of spatially registered images of fluorescence and surface-bound molecular density. Second, the use of a charge-coupled device (CCD) rather than laser scanning imaging simplifies the optical setup and enables large-area, high-resolution and high-throughput analysis. Third, a high-resolution motorized gimbal-mounted mirror and beam-expanded laser provide efficient and selective light coupling to the PC, especially crucial for the narrow resonances that provide optimal fluorescence enhancement and sensitive LF detection. Lastly, other imaging techniques available on the microscope, including reflected brightfield and differential interference contrast, can be overlaid with EF and LF images.

For LF imaging, the laser passes through the neutral density filter, rotating diffuser, and a blank in the filter wheel on the fluorescence microscope. A custom data acquisition and control program (LabView, National Instruments) translates the motorized mirror mount over a small range of angles and captures a single image for each discrete illumination angle. The resonant angle is computed for each pixel in the image stack by fitting the transmission versus angle data with a Lorentzian lineshape and finding the resonant angle. This resonant angle map is the LF image and can be used to quantify and visualize surface-bound density, as well as to find the appropriate resonant angle for EF imaging. The EF mode is generally used without the neutral density filter, without the rotating diffuser, and with an appropriate fluorescence filter set centered at 690 nm to match the Cy5 spectral emission maximum. For EF imaging, the desired angle of illumination is set in the control software and single images, sequences, or video can be captured.

#112354 - $15.00 USD Received 5 Jun 2009; revised 9 Jul 2009; accepted 11 Jul 2009; published 17 Jul 2009

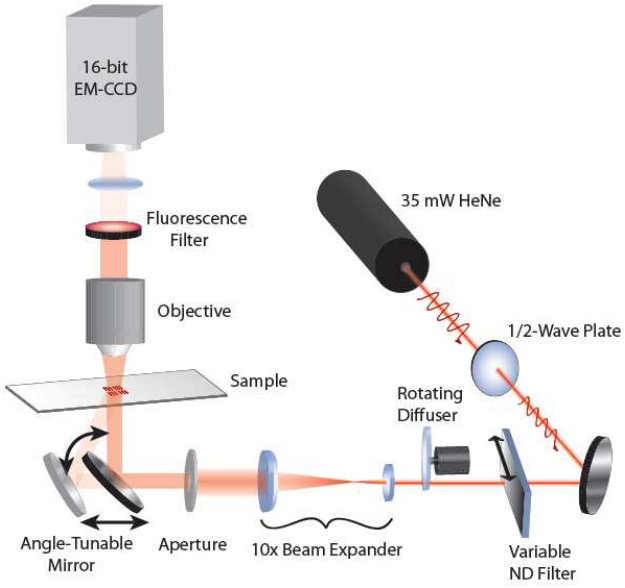

Fig. 1. Combined enhanced-fluorescence and label-free imaging instrument schematic.

The PC used in this study is shown schematically in Fig. 2(a) and is fabricated using a nanoreplica molding approach that has been described in detail previously [30]. Briefly, a silicon wafer with a "master pattern" etched into the surface is fabricated using deep-UV lithography and reactive ion etching to produce a negative surface volume image of the desired grating pattern for the finished sensor. A liquid UV-curable epoxy (UVCP) is sandwiched between a polyethylene terephthalate (PET) sheet and the silicon master wafer, and is subsequently cured using a high intensity UV lamp. The hardened epoxy adheres to the PET and is peeled away from the master, after which it is coated with SiO_2 to bias the high intensity fields in the high refractive index layer away from the autofluorescent polymers underneath. A TiO_2 high refractive index layer is then sputtered on to the device. An atomic force microscope surface profile of the replicated structure before dielectric deposition is shown in Fig. 2(b). Excellent uniformity of the low-cost replication process across very large areas enables incorporation of these devices into standardized formats such as microscope slides and micro-well plates. The devices used in this study are cut to the size of a 25x75 mm glass slide and adhered to this substrate with optical adhesive.

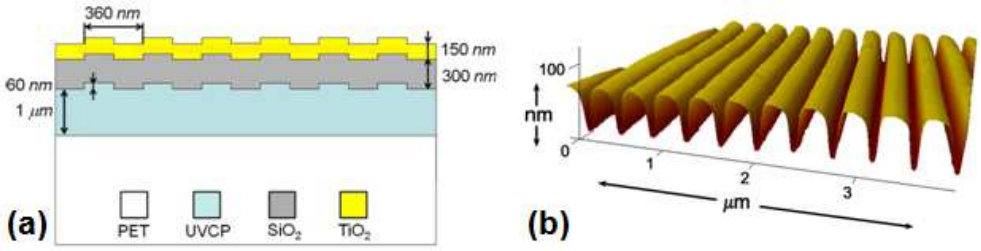

Fig. 2. Schematic (a) and atomic force microscope surface profile (b) of photonic crystal structure designed for label-free and enhanced-fluorescence imaging.

In order to maximize sensitivity for both LF and EF imaging, the PC device and instrument must work together in concert. The PC was optimized using rigorous coupled-

#112354 - $15.00 USD Received 5 Jun 2009; revised 9 Jul 2009; accepted 11 Jul 2009; published 17 Jul 2009

wave analysis (RCWA, RSoft Design) to meet several criteria. First, a resonant mode for near-normal incidence illumination at the HeNe wavelength (632.8 nm) must be engineered such that wide-field low numerical aperture (NA) objectives can be used for LF imaging. However, the resonant angle must not lie too close to normal incidence because LF sensitivity is lost very close to normal incidence due to band-flattening in the PC dispersion. The resonance should operate in TM polarization since this maximizes LF sensitivity [31]. This mode can also be used for resonant excitation of Cy5 as spectrally narrow resonances are desirable for optimizing both LF and EF performance. To facilitate maximum efficiency of the enhanced extraction effect, the PC must support a resonance centered spectrally at the Cy5 emission maximum (~690 nm) and spatially at the device normal [28]. In order to meet all of these criteria, RCWA simulation results stipulated the use of a 360 nm period structure with a step height of 60 nm coated with 300 nm of SiO_2 and 150 nm of TiO_2. The PC dispersion (or band diagram) measured from the fabricated device in transmission is shown for both TM and TE polarization in Fig. 3(a) and (b), respectively. TM and TE are defined for incident light polarized with the electric field parallel and perpendicular to the direction of the PC periodic modulation, respectively.

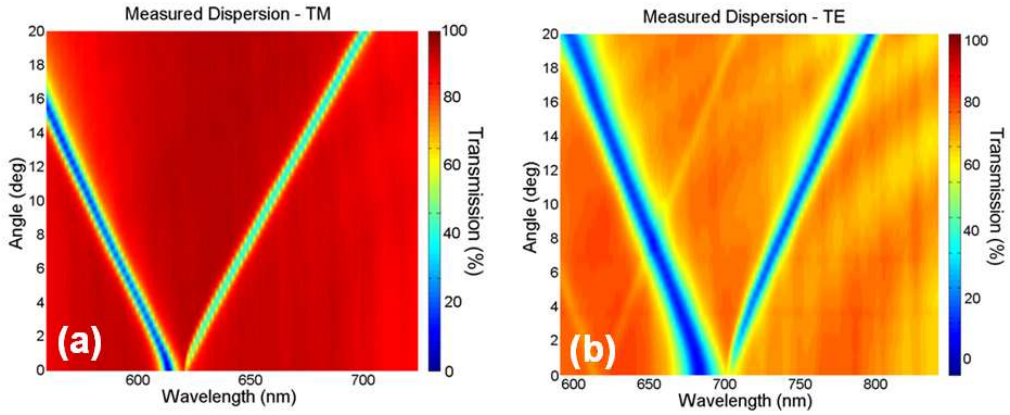

Fig. 3. Dispersion for (a) TM and (b) TE illumination of the PC used in this study. Resonance for label-free and enhanced excitation at 633 nm lies at ~2-deg in TM, while Cy5 emission can couple efficiently to TE resonant modes at 690 nm near the surface normal.

3. Enhanced-Fluorescence and Label-Free Imaging

Before biologically relevant experiments can be performed with a PC sensor, the surface must be functionalized with appropriate reactive groups. We chose to use a vapor-deposited monofunctional epoxysilane monolayer for its low autofluorescence, high density, and excellent uniformity [32]. The silane group provides covalent linkage to the surface oxide through free OH-groups, while the epoxide is highly reactive with proteins through the amino terminus or exposed lysine residues. Upon successful surface functionalization, 300 pL spots of strepavidin-cyanine-5 (SA-Cy5) at a range of concentrations from 50 μg/ml down to 24 ng/ml in 0.1% trehalose in PBS were deposited onto the PC using a non-contact piezoelectric spotting system (Perkin Elmer Piezorray). Following overnight incubation, the SA-Cy5 spots were washed in 0.1% Tween in PBS and then dH_20 with gentle agitation and subsequently dried under nitrogen.

#112354 - $15.00 USD Received 5 Jun 2009; revised 9 Jul 2009; accepted 11 Jul 2009; published 17 Jul 2009

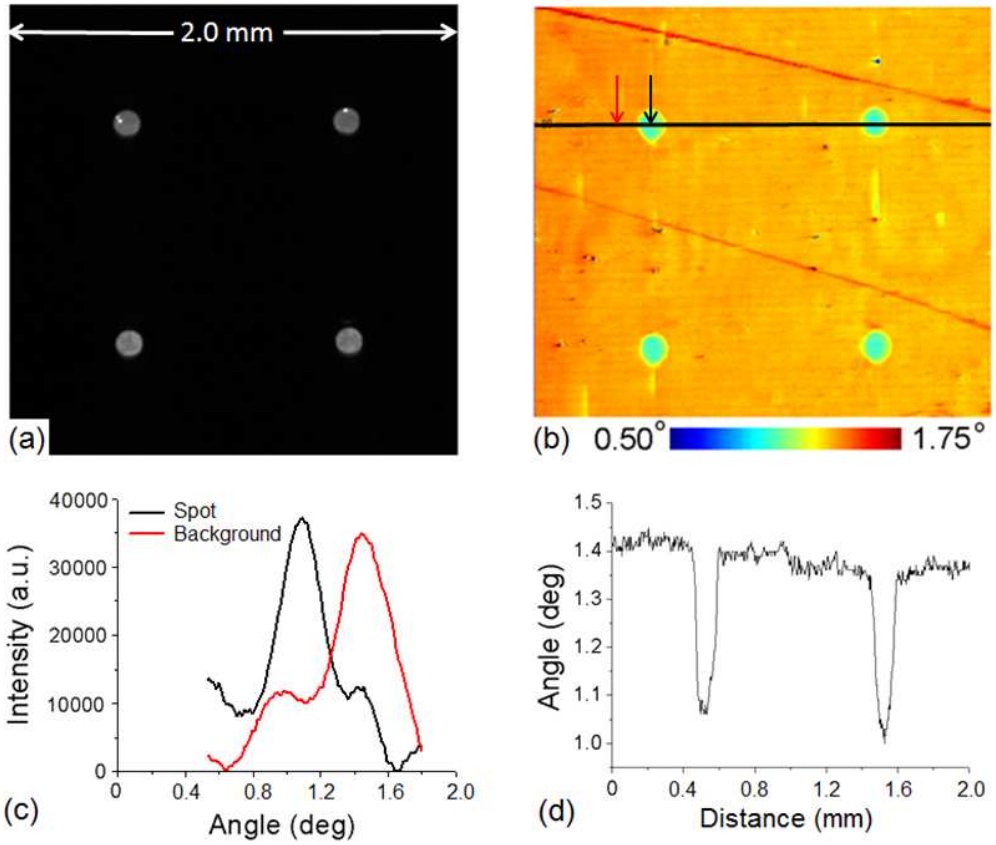

Fig. 4. Enhanced fluorescence (a) and label-free (b) images of 50 µg/ml SA-Cy5 spots on a PC. Inverted transmission versus angle response for a pixel inside and outside the SA-Cy5 spot (c) and cross-section of the label-free image through 2 SA-Cy5 spots(d).

A LF image was constructed by first imaging laser transmission through the SA-Cy5-immobilized PC for a range of angles, fitting the resonance profile pixel-by-pixel for 100 angles, and then generating a spatial map of the resonant angle across the imaged area. A 4x 0.10 NA objective (Olympus) was used to yield a 4 mm^2 imaged area. For each LF image captured, on-resonance fluorescence images were also gathered. Throughout this work, all fluorescence images are shade corrected in order to provide a flatter imaging field than that given by the uncorrected mild Gaussian profile characteristic of an expanded laser beam. Figs 4(a) and (b) show precise registration between the EF and LF images, respectively. Transmission data for a single-pixel angular response both inside and outside the spot of immobilized SA-Cy5 is plotted (inverted for fitting) in Fig. 4(c) while a line profile taken through the LF image is given in Fig. 4(d), both demonstrating robust LF image generation. LF response versus SA-Cy5 concentration is characterized in Fig. 5, where spot densities have been background corrected. The limit of detection (LOD) is set at three times the standard deviation of eight local background measurements taken in each quadrant around the perimeter of the regions immobilized with SA-Cy5. This is measured to be 25 mdeg of resonance angle shift and equal to the surface density resulting from the adsorption of SA-Cy5 from a ~2.5 µg/ml solution.

#112354 - $15.00 USD Received 5 Jun 2009; revised 9 Jul 2009; accepted 11 Jul 2009; published 17 Jul 2009

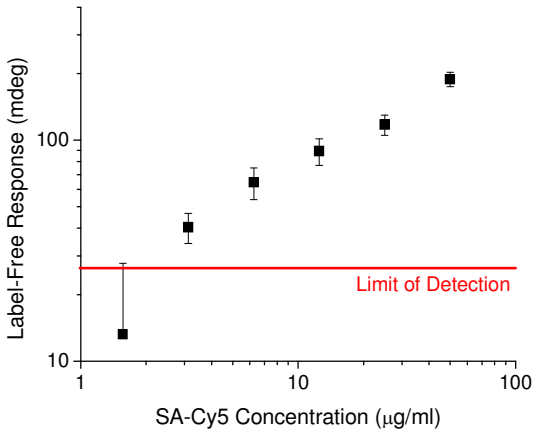

Fig. 5. Label-free response for two-fold dilution series of strepavidin-Cy5 spotted on a PC surface.

RCWA simulations, used previously to accurately predict PC biosensor sensitivity [31], were used here to determine the bulk refractive index change as well as the protein layer thickness change that correspond to the minimum resolvable change in resonance angle. Simulations reveal a corresponding bulk refractive index change of ~$5x10^{-4}$ or a 0.25 nm thickness change in an n_a=1.57 adsorbed layer, representative of a densely packed protein such as strepavidin [33]. While both of these figures are approximately 1 order of magnitude less sensitive than that reported for other methods including SPR imaging [34] and imaging ellipsometry [35, 36], it is dramatically hindered by the fact that there is no referencing performed here. Deterministic spatial variations in the resonance angle resulting from device imperfections and laser interference patterns are highly dominant over random noise sources including laser intensity fluctuations, photon statistics, and electronic readout noise. We are therefore currently working on implementing a motorized stage and image registration software in order to align and then subtract "before" and "after" label-free images from one another. Other label-free imaging implementations have demonstrated signal-to-noise ratio (SNR) improvements of more than an order of magnitude by implementing a referencing scheme [37], and so we anticipate comparable performance with the aforementioned techniques.

Table 1. Measured Photonic Crystal Fluorescence Enhancement

[SA-Cy5] (μg/ml)	Enhanced Excitation*	Enhanced Extraction†	Total Enhancement††
50	7.32	26.1	191
25	8.36	23.9	200
13	10.5	23.7	248
6.3	12.7	25.9	328

* Net spot intensity for PC on-resonance divided by net spot intensity for PC off-resonance

† Net spot intensity for PC off-resonance divided by net spot intensity for glass control

†† Net spot intensity for PC on-resonance divided by net spot intensity for glass control

#112354 - $15.00 USD Received 5 Jun 2009; revised 9 Jul 2009; accepted 11 Jul 2009; published 17 Jul 2009

Due to the large range of concentrations of spotted dye, fluorescence measurements of the twelve concentrations were imaged in three groups with distinct gain and exposure settings to maximize use of the 16-bit dynamic range of the CCD and minimize contributions from electronic noise sources. Fluorescence images were captured from the PC as well as from a standard glass slide that was processed alongside the PC as a control. By setting image gain, exposure and resonant illumination conditions constant between the PC and glass slide control, enhancement of up to 328x (for the 6.3 μg/ml SA-Cy5 spots) was measured. This figure is ~20x greater than that typically reported for plasmon-assisted enhancement [38, 39], ~10x greater than that published for planar reflective surfaces [40], and ~5x larger than PC enhancement measured with a commercial fluorescence scanner [27]. Table 1 summarizes the measured fluorescence enhancement for the highest four concentrations of SA-Cy5 and separates the individual effects of enhanced excitation (measured as the ratio of fluorescence intensities for the PC illuminated on- versus off-resonance) and enhanced extraction (measured as the ratio of fluorescence intensities for the PC off-resonance versus the glass slide control). The trend of decreasing enhanced excitation for higher concentrations arises because the local resonance angle of the 6.3 μg/ml spots was used as the illumination angle for the on-resonance case. Due to the narrow angular linewidth of the resonance used here (full-width at half-max = 0.3º) and because the local resonance angle varies significantly between concentrations for these high-density spots (as Fig. 5 illustrates), variability in the enhanced excitation response is expected. However, enhanced excitation uniformity is substantially better when the spot density variability is more representative of the targeted biological applications.

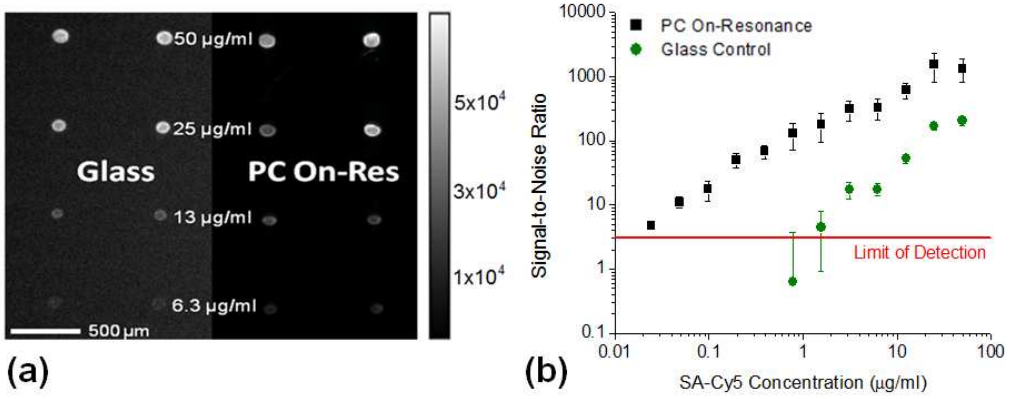

Fig. 6. (a) Gain and exposure-optimized images of SA-Cy5 fluorescence on glass compared to PC EF. (b) Signal-to-noise vs SA-Cy5 concentration showing over two orders of magnitude improvement in limit of detection (LOD).

The PC provides not only substantial increases in fluorescence output, but also much more importantly, significant reductions in the fluorescence detection limit. In order to demonstrate this, individually gain/exposure-optimized fluorescence images were captured for the PC illuminated on-resonance and for the glass slide and are shown side-by-side in Fig. 6(a). As a more appropriate performance metric for fluorescence-based assays (as opposed to raw intensity enhancement numbers), SNRs are calculated from the optimized images for each SA-Cy5 concentration spotted onto the PC and glass slide and are shown in Fig. 6(b). The signal is background subtracted and noise is defined as the standard deviation of eight local background measurements taken in each quadrant around the perimeter of each spot. As defined previously for the LF measurements, the LOD is set for a SNR of three. SNR enhancement for the PC is 41x for the lowest detectable concentration (1.5 μg/ml) on the glass slide, and the LOD is reduced by more than two orders of magnitude.

#112354 - $15.00 USD Received 5 Jun 2009; revised 9 Jul 2009; accepted 11 Jul 2009; published 17 Jul 2009

4. Application to DNA Microarrays

In order to demonstrate the potential utility of combined EF and LF imaging, a DNA microarray experiment was carried out on PC and control glass slides. PC slides were functionalized with (3-glycidoxypropyl)trimethoxysilane at 185 mTorr overnight, and were run in the experiment in parallel with commercially available glass microarray slides (Corning UltraGAPS). Both PCs and glass slides were spotted with a set of 192 different 70mer oligonucleotide sequences representative of known *Glycine max* genes. Using a QArray^2 (Genetix) contact pin-spotter, slides were spotted with 40 replicates per oligo for a total of 7680 spots on a single slide. After rinsing unbound DNA from the array, LF images of the immobilized 70mers were captured. The LF images shown in Fig. 6(a) and (b) illustrate the robust signals generated by DNA binding. GenePix Pro microarray analysis software (Molecular Devices) was used to calculate the background-subtracted label-free resonance shift for spots on the array. For the 64 spots shown, the average resonance angle shift is 380 ± 65 mdeg, giving a coefficient of variation (CV) of 17.2% across the imaging area. The spot density variation across 400 spots on this microarray as measured with LF imaging was calculated to be 22.2%. The mild smearing towards the spot edges in the horizontal direction is a result of small but finite propagation lengths associated with the resonant modes. After LF imaging, RNA was extracted from *Glycine max* cotyledon, and reverse transcriptase labeled with Cy-5. Identical labeled samples were hybridized to PCs and glass slides for 16 hrs at 42° C. An EF image of the hybridized array, registered precisely to the area previously captured with LF imaging, is shown in Figs. 6(c) and (d).

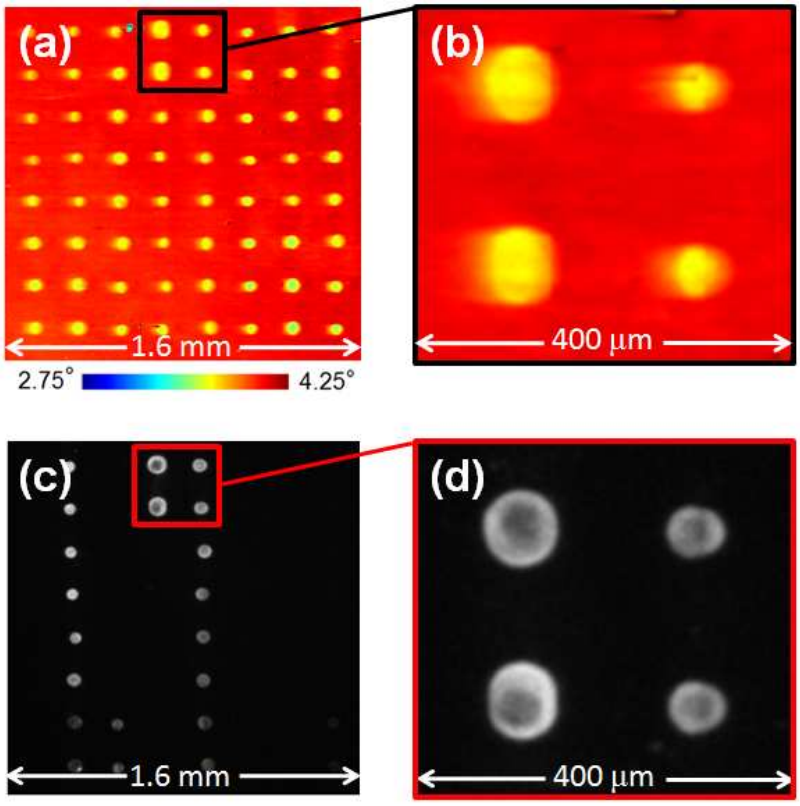

Fig. 6. Label-free image of spotted 70mer capture DNA(a) and enlarged view of four spots (b). Enhanced-fluorescence image of the same area after sample hybridization (c) and enlarged view of the same four spots (d).

#112354 - $15.00 USD Received 5 Jun 2009; revised 9 Jul 2009; accepted 11 Jul 2009; published 17 Jul 2009

Comparing fluorescence images on the PC to those captured on the control glass slide allows for a clear demonstration of the significant fluorescence enhancement that can be achieved for DNA microarrays using the instrumentation and PCs described and characterized in this work. Fig 7(a) shows an EF image of an area containing 64 spots where the laser illumination has been aligned to the resonance angle. A second image was captured of the same area for laser illumination several set degrees off of the resonance angle (not shown). Fig. 7(b) contains a third image that was captured of the same array pattern on a glass slide substrate. The spot size variation between the glass and PC surface is due to differences in the hydrophobicity between the commercially and laboratory prepared surface chemistries. Gain and exposure settings were held constant for the acquisition of these three images. Registered cross section profiles through five replicate spots are given for the three devices in Fig. 7(c), demonstrating 11.5x excitation enhancement (from off to on-resonance on the PC) and 9.3x extraction enhancement (from the glass slide to the PC illuminated off-resonance). The effects of these multiply to provide up to 109x total fluorescence enhancement (from glass slide to PC on-resonance).

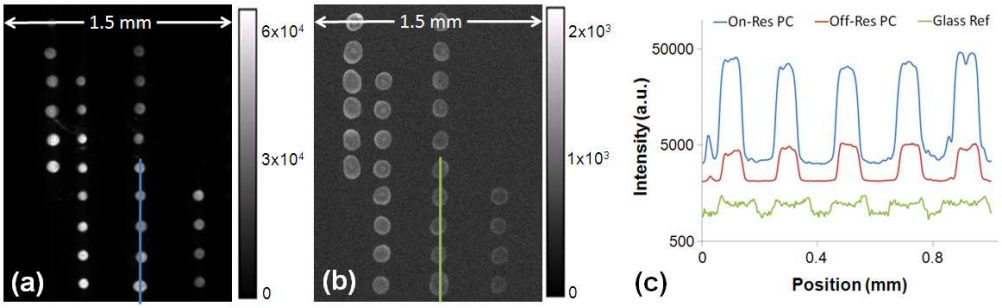

Fig. 7. Fluorescence image of hybridized DNA microarray on a PC illuminated on-resonance (a) and on a control glass slide (b). Intensity cross-sections through five replicate spots for the PC illuminated on-resonance, illuminated off-resonance, and for the glass slide (c).

While the raw increase in collected fluorescence is considerable, it is certainly possible to adjust the gain and exposure settings of the CCD such that the total number of photons emitted by the fluorescent spots that reach the detector is the same. In a similar fashion to that done previously for the SA-Cy5 sensitivity characterization assay, the exposure time for the glass slide was increased by 11 times, as this is the additional intensity available on the PC due to the enhanced excitation mechanism. The CCD gain was then increased to fill the dynamic range of the 16-bit camera and match raw spot intensities with those on the PC as closely as possible. Fluorescence images of the labeled, hybridized DNA on the PC and glass slide are given in Fig. 8(a) and (b), respectively. The same software as used for LF analysis is employed here to calculate net spot intensities and a global background noise figure. Spots having an SNR greater than three are plotted versus array location in Fig. 8(c). Three times as many genes on the PC versus the glass slide exceed this detection limit.

#112354 - $15.00 USD Received 5 Jun 2009; revised 9 Jul 2009; accepted 11 Jul 2009; published 17 Jul 2009

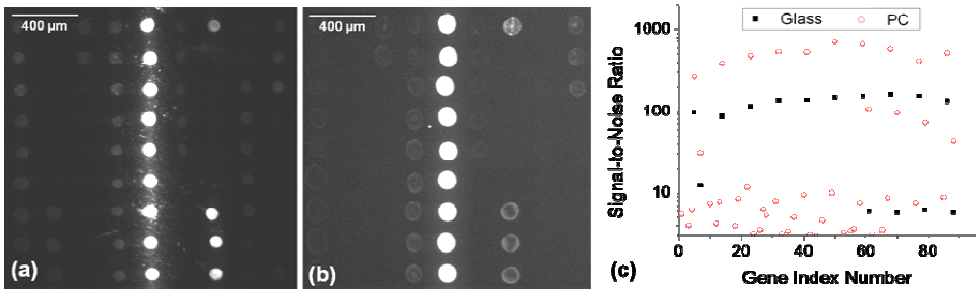

Fig. 8. Exposure and gain-optimized fluorescence images of hybridized DNA microarray on a PC illuminated on-resonance (a) and on a control glass slide (b). (c) Signal-to-noise ratio (SNR) of spots exceeding an SNR of 3 are plotted versus spot location in the array for each image.

5. Discussion

The imaging instrument presented in this work has been designed to take full advantage of the EF and LF mechanisms afforded by PC surfaces. The collimated narrow-bandwidth illumination source and fine incidence-angle tuning enable efficient coupling to the narrow PC resonances that are ideal for both EF and LF imaging. The LF imaging technique enables both independent biodetection as well as precise determination of the optimal resonance angle for subsequent EF illumination. The full decoupling of the illumination and imaging optics allows independent optimization of both optical paths. The computer-controlled tunable mirror determining the illumination angle can closely track excitation resonance locations while the numerical aperture of the imaging objective provides a range of acceptance angles for directionally biased fluorescence from PC surface. These are crucial for obtaining maximum benefit from both enhanced excitation and enhanced extraction mechanisms.

For fluorescence detection of both directly spotted SA-Cy5 and hybridized Cy5 reverse transriptase labeled DNA, it is clear that PC EF generates significant improvements in the SNR for each assay. There are three mechanisms by which PC EF yields gains in SNR. First, enhanced excitation produces strong optical near-fields that can excite surface-bound fluorophores at a greater rate than can the uncoupled incident illumination. This effect is similar to using a more powerful laser for illumination, but with the benefits of avoiding the additional cost and bulk, if one is available at all. Second, enhanced extraction selectively redirects fluorescence emission towards the detector, maximizing the efficiency of fluorescence collection. This effect is similar to using a very high numerical aperture objective and immersion media, though with greatly reduced cost, complexity, and sample format limitations. These first two mechanisms both achieve SNR improvements through photon statistics and/or a reduction in the CCD dark current and excess noise factor by minimizing image exposure time and gain levels, respectively. The third benefit of PC EF is that it is inherently confocal. Fluorophores residing near the PC device surface are preferentially excited by enhanced fields while their emission is selectively funneled towards the detector by careful engineering of the photonic crystal dispersion. Substrate autofluorescence, the primary noise source of a bare PC or glass substrate, is excited with only weak non-enhanced incident illumination while the emission does not significantly couple to resonant PC modes and therefore has a more traditional angular emission profile. This selective excitation and energy extraction enables significantly greater fluorescence imaging sensitivity than is achievable with a conventional wide-field microscope.

A soybean microarray has been used in this work to showcase these benefits of PC EF as well those of registered LF imaging, both using the single optical system described here. While DNA microarrays have gained widespread adoption over the past 10-15 years in life

#112354 - $15.00 USD Received 5 Jun 2009; revised 9 Jul 2009; accepted 11 Jul 2009; published 17 Jul 2009

science and medical research, the highly multiplexed nature of the platform presents particularly difficult challenges in controlling uniformity across tens of thousands of spots and optimizing sensitivity to genes present at magnitudes spanning many orders of magnitude [41]. In this work we have presented a proof-of-concept to address these major limitations. We have shown the ability to image the density of immobilized probe DNA with sufficient resolution and sensitivity to clearly observe variations in spotted density, size and shape. Given that hybridization kinetics are strongly influenced by immobilized DNA density [42] and spot size [43], label-free imaging can be used to screen for missing or bad spots or to potentially adjust the hybridized fluorescence signals accordingly. In addition, we have used the EF mechanisms to improve the sensitivity of imaging fluorescently-tagged hybridized DNA. This ability to more sensitively detect hybridized DNA can lead to the identification of disease-associated genes that may have previously gone undetected. In the context of human genomics, this additional information could aid researchers and clinicians in disease pathway discovery and earlier detection diagnostics. Furthermore, the enhanced quality control afforded by LF DNA capture probe imaging can provide more accurate data and can reduce cost and processing time by limiting the number of experimental replicates.

6. Conclusions

We have reported on the design of an imaging system optimized for EF detection and registered LF image acquisition. Using microspots of SA-Cy5 on PC surfaces to characterize the instrument, we have demonstrated raw signal enhancement of 328x and SNR enhancement of 41x. These dramatic improvements over glass slide-based measurements show the ability of the EF/LF imaging instrument to optimally interface with an engineered PC surface. LF images of a *Glycine max* microarray printed on a PC illustrate the potential of this method for quality control of the immobilized capture DNA spots. EF images of this same area of the array enable detection of 3x more genes in the sample than for a glass slide.

Acknowledgements

This work was supported by SRU Biosystems, the National Science Foundation (CBET 07-54122), and the National Institutes of Health (PHS 1 R01 CA118562). Any opinions, findings, and conclusions or recommendations expressed in this material are those of the authors and do not necessarily reflect the views of the National Science Foundation. The authors would like to thank colleagues from the Nano Sensors Group for their suggestions and input.

Contact

* B.T. Cunningham, tel: +1-217-265-6291; bcunning@illinois.edu

#112354 - $15.00 USD Received 5 Jun 2009; revised 9 Jul 2009; accepted 11 Jul 2009; published 17 Jul 2009